Mon. Not. R. Astron. Soc. **000**, 1–10 (2013) Printed 30 July 2014 (MN LATEX style file v2.2)

Discovery of extremely lead-rich subdwarfs: does heavy metal signal the formation of subdwarf B stars?

Naslim N.[1,2⋆], C. S. Jeffery[1]†, A. Hibbert[1,3], and N. T. Behara[1,4]
[1] *Armagh Observatory, College Hill, Armagh BT61 9DG*
[2] *Institute of Astronomy and Astrophysics, Academica Sinica P.O Box 23-141, Taipei 10617, Taiwan R.O.C*
[3] *School of Mathematics, Queens University Belfast, Belfast BT7 1NN*
[4] *Institut d'Astronomie et d'Astrophysique, Université Libre de Bruxelles, B-1050 Bruxelles, Belgium*

arXiv:1407.7668v1 [astro-ph.SR] 29 Jul 2014

Accepted ..... Received ..... ; in original form .....

ABSTRACT

Hot subdwarfs represent a group of low-mass helium-burning stars formed through binary-star interactions and include some of the most chemically-peculiar stars in the Galaxy. Stellar evolution theory suggests that they should have helium-rich atmospheres but, because radiation causes hydrogen to diffuse upwards, a majority are extremely helium poor. Questions posed include: when does the atmosphere become chemically stratified and at what rate?

The existence of several helium-rich subdwarfs suggests further questions; are there distinct subgroups of hot subdwarf, or do hot subdwarfs change their surface composition in the course of evolution? Recent analyses have revealed remarkable surface chemistries amongst the helium-rich subgroup. In this paper, we analyse high-resolution spectra of nine intermediate helium-rich hot subdwarfs. We report the discovery that two stars, HE 2359–2844 and HE 1256–2738, show an atmospheric abundance of lead which is nearly ten thousand times that seen in the Sun. This is measured from optical Pb IV absorption lines never previously seen in any star. The lead abundance is ten to 100 times that measured in normal hot subdwarf atmospheres from ultraviolet spectroscopy. HE 2359–2844 also shows zirconium and yttrium abundances similar to those in the zirconium star LS IV−14°116. The new discoveries are interpreted in terms of heavily stratified atmospheres and the general picture of a surface chemistry in transition from a new-born helium-rich subdwarf to a normal helium-poor subdwarf.

Key words: star: chemically peculiar (helium) stars: evolution, stars: abundances, stars: horizontal-branch, stars: subdwarf, atomic data

1 INTRODUCTION

The formation of hot subdwarf B stars remains a puzzle; they are observed as single stars, and as both close and wide binaries. They are widely regarded to be core-helium burners; the majority have hydrogen-rich atmospheres, but this is only a thin veneer, since they behave as helium main-sequence or extended horizontal-branch stars of approximately half a solar mass (Heber 2009). The puzzle is that the majority are believed to be red-giant cores, stripped of their hydrogen envelopes, so at best their outer layers should be enriched in helium. Whilst the majority have helium-poor surfaces (helium number fraction $n_{\rm He} < 1\%$), a minority show helium-rich surfaces with a wide range of nitrogen and carbon abundances. It appears that in the "normal" (helium-poor) sdB stars, radiative levitation and gravitational settling cause helium to sink below the hydrogen-rich surface (Heber 1986), deplete other light elements, and enhance many heavy elements in the photosphere (O'Toole & Heber 2006).

It has been found that almost 10% of the total subdwarf population comprises stars with helium-rich atmospheres (Green et al. 1986; Ahmad & Jeffery 2006; Németh et al. 2012). These are sometimes referred to as He-sdB and He-sdO stars, depending on the ratios of certain He I and He II lines (Moehler et al. 1990; Ahmad & Jeffery 2004; Drilling et al. 2013) or more generally as helium-rich hot subdwarfs (He-sd's). A small number of these show a surface helium abundance in the range $n_{\rm He} \approx 5-80\%$. Naslim et al. (2012) suggested a terminology based on helium content. He-sd's with $n_{\rm He} > 80\%$ were described as extremely helium-

⋆ E-mail: naslimn@asiaa.sinica.edu.tw
† E-mail: csj@arm.ac.uk

rich, whilst those having $5\% < n_{\rm He} < 80\%$ were described as intermediate helium-rich. Since the numbers in both groups are small, the question naturally arises whether these are truly distinct classes, or simply a convenient description of an undersampled continuum. The corollary is whether the classes represent different stages in the evolution of similar objects, thus representing a gradual change in photospheric composition due to slow chemical separation, or represent objects with quite distinct origins.

The formation of the extreme-helium subdwarfs appears to be well explained by the merger of two helium white dwarfs (Zhang & Jeffery 2012). However, it is harder to understand the intermediate-helium subdwarfs; to date, few have been analyzed and those that have been are diverse. The latter include the prototype JL 87 (Ahmad et al. 2007), the zirconium star LS IV−14°116 (Naslim et al. 2011), the short period binary CPD−20°1123 (Naslim et al. 2012), and also UVO 0512–08 and PG 0909+276 (Edelmann 2003). They appear to occupy a region of effective-temperature – helium-abundance space which is almost unpopulated in the Németh et al. (2012) survey (Fig. 6). The question posed by these stars is whether they are related either to normal sdB stars or to extreme He-subdwarfs or to both. The question can be addressed by, *inter alia*, establishing whether the variation in chemical and/or binary properties across the three groups is discrete or continuous.

Although rare, a few apparently intermediate-helium subdwarfs were identified and partially analysed in the course of the ESO Supernova Ia Progenitor surveY (SPY) (Napiwotzki et al. 2001; Lisker et al. 2004; Ströer et al. 2007; Hirsch & Heber 2009). Our present objective was to analyse nine SPY He-sd's in greater detail and attempt to answer the question just posed.

2 OBSERVATIONS

The ESO SPY (Napiwotzki et al. 2001) obtained VLT/UVES spectra for 76 sdB/sdOB and 58 sdO stars (Lisker et al. 2004) which had been identified as white dwarf candidates mostly from the Hamburg ESO survey (Christlieb et al. 2001). Reduced high-resolution spectra were obtained from the ESO UVES archive (Ballester et al. 2000) for HE 0111–1526, HE 1135–1134, HE 1136–2504, HE 1238–1745 HE 1256–2738, HE 1258+0113, HE 1310–2733, HE 2218–2026 and HE 2359–2844. These had been indentified as having $0.05 < n_{\rm He} < 0.90$ by Ströer et al. (2007). For each star at least two spectra were available with signal-to-nose ratios between 26 and 31 in the continuum. For abundance analysis we selected the wavelength range 3600 – 5000 Å. The UVES spectra of all nine intermediate He-sds display strong lines of interesting ions.

Carbon. HE 2359–2844, HE 0111–1526, HE 2218–2026 and HE 1256–2738 show strong CII and CIII lines. No carbon lines were identified in HE 1310–2733, HE 1135–1134, HE 1136–2504, HE 1238–1745 and HE 1258+0113.

Zirconium. Naslim et al. (2011) reported zirconium and yttrium lines in LS IV−14°116. The same ZrIV and YIII lines along with two more ZrIV lines at 3687 and 3764 Å are found in HE 2359–2844.

Lead. The UVES spectrum of HE 2359–2844 shows a strong absorption line at 4049.8Å and weaker lines at 3962.5 and 4496.1Å. These have been identified from the NIST atomic database to be due to Pb IV (Kramida et al. 2012). HE 1256–2738 also shows the Pb IV 4049.8Å line and 3962.5; 4496.1Å is too weak to measure. To our knowledge, these lines have not been observed in any other astronomical object, although O'Toole (2004) identified PbIV lines in Space Telescope ultraviolet spectra of the sdB stars Feige 48 and PG1219+534.

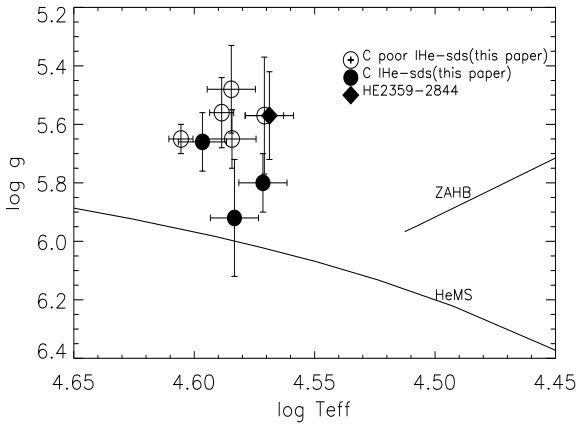

Figure 1. $T_{\rm eff}$ and $\log g$ for nine intermediate He-subdwarfs measured for this paper. Symbols distinguish carbon-rich and carbon-poor stars, as well as the zirconium star HE 2359–2844. Approximate locations for the helium main sequence and the zero-age horizontal branch are also shown.

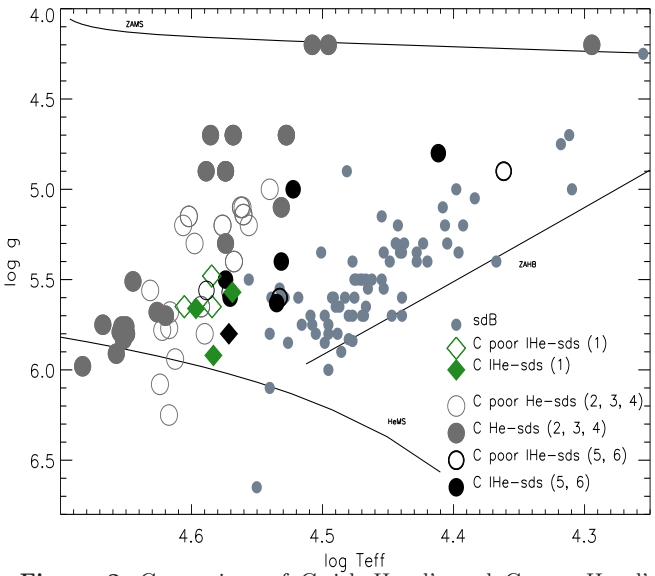

Figure 2. Comparison of C-rich He-sd's and C-poor He-sd's in a $T_{\rm eff}$-$\log g$ plane. The hot subdwarfs shown in this figure include 1. Intermediate He-sd's discussed in this paper, 2. He-sd's fromNaslim et al. (2010), 3. Intermediate He-sd's from Naslim et al. (2011), 4. He-sdO's from Ströer et al. (2007), 5. He-sd's from Ahmad & Jeffery (2003), and normal sdBs from Edelmann et al. (2003).

Table 1. Atmospheric parameters

Star	$T_{\rm eff}$(K)	$\log g$	$n_{\rm He}$	y	$v \sin i$ (km s^{-1})	Source
HE 0111–1526	38 310 ± 1200	5.93 ± 0.2	0.80 ± 0.12	4.0 ± 0.6	3 ± 1	SFIT
	39 152	6.31	0.87			1
HE 1135–1134	38 400 ± 1500	5.65 ± 0.1	0.36 ± 0.15	0.56 ± 0.23	2 ± 1	SFIT
	40 079	5.68	0.35			1
HE 1136–2504	40 320 ± 500	5.65 ± 0.05	0.49 ± 0.19	0.96 ± 0.37	3 ± 2	SFIT
	41 381	5.84	0.40			1
HE 1238–1745	37 230 ± 800	5.57 ± 0.2	0.28 ± 0.05	0.39 ± 0.07	8 ± 2	SFIT
	38 219	5.64	0.22			1
HE 1256–2738	39 500 ± 1000	5.66 ± 0.1	0.49 ± 0.19	0.96 ± 0.37	4 ± 1	SFIT
	40 290	5.68	0.55			1
HE 1258+0113	38 780 ± 500	5.56 ± 0.12	0.25 ± 0.1	0.33 ± 0.13	5 ± 1	SFIT
	39 359	5.64	0.23			1
HE 1310–2733	38 400 ± 1100	5.48 ± 0.15	0.44 ± 0.15	0.79 ± 0.27	6 ± 2	SFIT
	40 000	5.63	0.41			1
HE 2218–2026	37 280 ± 1500	5.8 ± 0.1	0.30 ± 0.1	0.43 ± 0.14	10 ± 3	SFIT
	38 330	5.87	0.31			1
HE 2359–2844	37 050 ± 1000	5.57 ± 0.15	0.43 ± 0.18	0.75 ± 0.32	5 ± 2	SFIT
	38 325	5.65	0.42			1

Reference: 1. Ströer et al. (2007)

3 ATMOSPHERIC PARAMETERS

We measured effective temperature $T_{\rm eff}$, surface gravity $\log g$, and helium abundance $n_{\rm He}$ by fitting He I and Balmer lines using the χ^2-minimization package SFIT (Jeffery & Aznar Cuadrado 2001). The observed spectra were matched to a grid of *fully* line-blanketed models computed in local-thermodynamic and hydrostatic equilibrium using opacity-sampling and a linelist of some 10^6 transitions (Behara & Jeffery 2006). The grid covers a wide range in $T_{\rm eff}$, g, and $n_{\rm He}$ for a number of distributions of elements heavier than helium, including solar, 1/10 solar and other custom-designed mixtures (Behara & Jeffery 2006). For this analysis we sought solutions in the range $34\,000 < T_{\rm eff}/{\rm K} < 50\,000$, $4.5 < \log g(cgs) < 6.0$ and $0.10 < n_{\rm He} < 0.90$ over the wavelength interval $3600 - 5000$Å. A microturbulent velocity of $v_{\rm t} = 10\,{\rm km\,s^{-1}}$ was adopted, as determined for other He-sdBs by Naslim et al. (2010), where other details of the fitting procedure can also be found. The SFIT parameters $T_{\rm eff}$, $\log g$, $n_{\rm He}$ and $v \sin i$ (an upper limit to the projected rotational velocity) for each star are shown in Table 1, and also in Fig. 1. Errors given in Table 1 are formal errors from the χ^2 solution. $y \equiv n_{\rm He}/n_{\rm H}$ is also included.

Since the measured values of $T_{\rm eff}$ lie close to $\approx 40\,000$K, the increasing importance of departures from local thermodynamic equilibrium (LTE) needs to be considered and, in any case, our results should be compared with those obtained by Ströer et al. (2007). The latter used a grid of partially line-blanketed non-LTE model atmospheres calculated using the code PRO2 (Werner 1986; Werner et al. 2003). It remains to be seen whether the incompleteness of line-blanketing is more or less significant than departures from LTE for the stars considered here. Our $T_{\rm eff}$ are systematically cooler by ≈ 1200 K and our gravities are systematically weaker by ≈ 0.1 dex than those of Ströer et al. (2007), but the helium abundances are in almost complete agreement. This gives some confidence in the abundances derived for other species using our models. The systematic increase in the logarithmic abundance of Pb IV due to an increase in $T_{\rm eff}$ of 2 000 K is +0.12 for HE2359–2844 and –0.12 for HE1256–2738.

4 ABUNDANCES

For abundance measurements the grid model atmospheres closest to the measured $T_{\rm eff}$, $\log g$, and $n_{\rm He}$ and 1/10 solar metallicity were adopted. After measuring the equivalent widths of all C, N, O, Mg, Al, Si, and S lines using the spectrum analysis tool DIPSO, the individual line abundances were calculated using the LTE radiative transfer code SPECTRUM (Jeffery et al. 2001).

Mean abundances for each element are given in Table 2. Abundances are given in the form $\epsilon_i = \log n_i + c$ where $\log \Sigma_i a_i n_i = 12.15$ and a_i are atomic weights. This form conserves values of ϵ_i for elements whose abundances do not change, even when the mean atomic mass of the mixture changes substantially. The errors given in Table 2 are based on the standard deviation of the line abundances about the mean or, in the case of a single representative line, on the estimated error in the equivalent width measurement. The elemental abundances shown in Table 2 are the mean abundances of all individual lines of an ion. Abundances for two other intermediate He-sds JL 87 and LS IV−14°116 are also shown.

In HE 2359–2844, HE 0111–1526, HE 2218–2026 and HE 1256–2738, carbon is nearly solar or slightly over abundant, while only upper limits to carbon abundances can be measured for HE 1310–2733, HE 1135–1134, HE 1136–2504, HE 1238–1745 and HE 1258+0113. In all nine stars, silicon appears to be underabundant relative to solar. Where detectable, sulphur and magnesium are relatively normal. Upper limits were estimated for several elements by assuming that, where no lines of a given ion could be measured, the

Table 2. Elemental abundances in the form $\epsilon_i = \log n_i + c$ (see text). The numbers of lines used in each measurement are shown in parentheses.

Star	H	He	C	N	O	Ne	Mg	Si	S
HE 0111–1526	10.88	11.48	8.49 ± 0.23 (18)	8.42 ± 0.38 (20)	< 6.9	7.51 ± 0.23 (6)	6.98 ± 0.10 (1)	6.79 ± 0.31 (7)	6.94 ± 0.11 (2)
HE 1135–1134	11.67	11.42	< 6.5	8.19 ± 0.46 (8)	< 7.4	< 7.0	< 6.5	< 6.1	< 6.4
HE 1136–2504	11.45	11.44	< 7.1	8.22 ± 0.33 (12)	< 7.5	< 7.1	< 6.5	< 6.1	< 6.6
HE 1238–1745	11.72	11.31	< 6.4	8.09 ± 0.40 (11)	< 7.3	< 7.0	< 6.5	5.97 ± 0.12 (2)	6.97 ± 0.12 (2)
HE 1256–2738	11.45	11.44	8.90 ± 0.54 (17)	8.14 ± 0.62 (10)	8.08 ± 0.1 (3)	< 7.1	< 6.5	6.19 ± 0.10 (2)	< 6.5
HE 1258+0113	11.74	11.26	< 6.9	7.59 ± 0.42 (5)	< 7.4	< 7.0	< 6.5	< 6.0	< 6.4
HE 1310–2733	11.49	11.39	< 6.8	8.29 ± 0.28 (18)	< 7.3	7.76 ± 0.1 (5)	7.76 ± 0.09 (1)	6.80 ± 0.08 (6)	6.81 ± 0.05 (2)
HE 2218–2026	11.60	11.22	8.81 ± 0.83 (9)	< 7.2	< 7.5	< 7.1	< 6.5	< 6.1	< 6.5
HE 2359–2844	11.58	11.38	8.51 ± 0.29 (15)	8.00 ± 0.57 (9)	7.81 ± 0.16 (5)	< 6.9	7.6 ± 0.1	5.73 ± 0.13 (2)	< 6.3
JL 87[1]	11.62 ± 0.07	11.26 ± 0.18	8.83 ± 0.04	8.77 ± 0.23	8.6 ± 0.23	8.31 ± 0.57	7.36 ± 0.33	7.22 ± 0.27	6.88 ± 1.42
LS IV−14°116[2]	11.83	11.23 ± 0.05	8.04 ± 0.22	8.02 ± 0.2	7.6 ± 0.17	< 7.6	6.85 ± 0.1	6.32 ± 0.12	
Sun[3]	12.00	[10.93]	8.43	7.83	8.69	[7.93]	7.60	7.51	7.12

References: 1. Ahmad et al. (2007), 2. Naslim et al. (2011), 3. Asplund et al. (2009); photospheric abundances except helium (helioseismic) and neon.

Table 3. Abundances derived for Zr IV, Y III, Pb IV in HE 2359–2844 and Pb IV in HE 1256–2738.

Ion λ/Å	Configuration	E_i/eV	$\log gf$	HE 2359–2844 w_λ/mÅ	 ϵ_i	HE 1256–2738 w_λ/mÅ	 ϵ_i	LS IV−14°116 ϵ_i [3]	Sun ϵ_i [6]
Zr IV									
3686.905	$6p^2P_{3/2} - 6d^2D_{5/2}$	21.17[1]	+0.746[3]	66	6.36				
3764.319	$6d^2D_{5/2} - 6f^2F_{7/2}$	24.51	+0.485[3]	26	6.61				
4198.265	$5d^2D_{5/2} - 6p^2P^0_{3/2}$	18.23	+0.323[4]	86	6.32				
4317.081	$5d^2D_{3/2} - 6p^2P^0_{1/2}$	18.18	+0.069[4]	64	6.60				
				mean	6.47			6.53	2.58
					±0.15			±0.24	±0.04
Y III									
4039.602	$4f^2F_{7/2} - 5g^2G_{9/2}$	12.53[2]	+1.005[3]]	42	6.60				
4039.602	$4f^2F_{7/2} - 5g^2G_{7/2}$	12.53	−0.538[3]]						
4040.112	$4f^2F_{5/2} - 5g^2G_{7/2}$	12.53	+0.892[4]	35	6.63				
				mean	6.61			6.16	2.21
					±0.15			±0.10	±0.04
Pb IV									
3962.48	$6d^2D_{3/2} - 5d^96s6p[16^o]_{1/2}$	22.88[5]	−0.047[5]	15	5.45	42	6.56		
4049.80	$7s^2S_{1/2} - 5d^96s6p[16^o]_{1/2}$	22.94	−0.065	25	5.74	68	6.23		
4496.15	$6d^2D_{5/2} - 5d^96s6p[15^o]_{3/2}$	23.16	−0.237	15	5.73				
				mean	5.64		6.39		1.75
					±0.16		±0.23		±0.10

References: 1. Reader & Acquista (1997), 2. Epstein & Reader (1975), 3. Naslim et al. (2011), 4. this paper, 5. Safronova & Johnson (2004), 6. Asplund et al. (2009).

equivalent width of the strongest lines due to that ion between 4000 and 5000 Å were less than 5 mÅ.

The Zr IV and Pb IV lines in HE 2359–2844, together with best-fit theoretical spectra, are shown in Figs. 3 and 4. The C II,III and Pb IV 3962.48, 4049.80 lines in the spectrum of HE 1256–2738, along with the best fit theoretical spectrum are shown in Fig. 5. Pb IV 4496.2 is not seen in HE1256-2738 because of the lower signal-to-noise of that spectrum. Pb IV 4534.6 and 4605.4 lie in a gap between two sections of the UVES spectrum.

Individual line abundances for ytttrium, zirconium and lead for both stars are given in Table 3. These are all nearly 4 dex above solar. A comparison of abundances relative to solar values for both lead-rich stars and LS IV−14°116 is

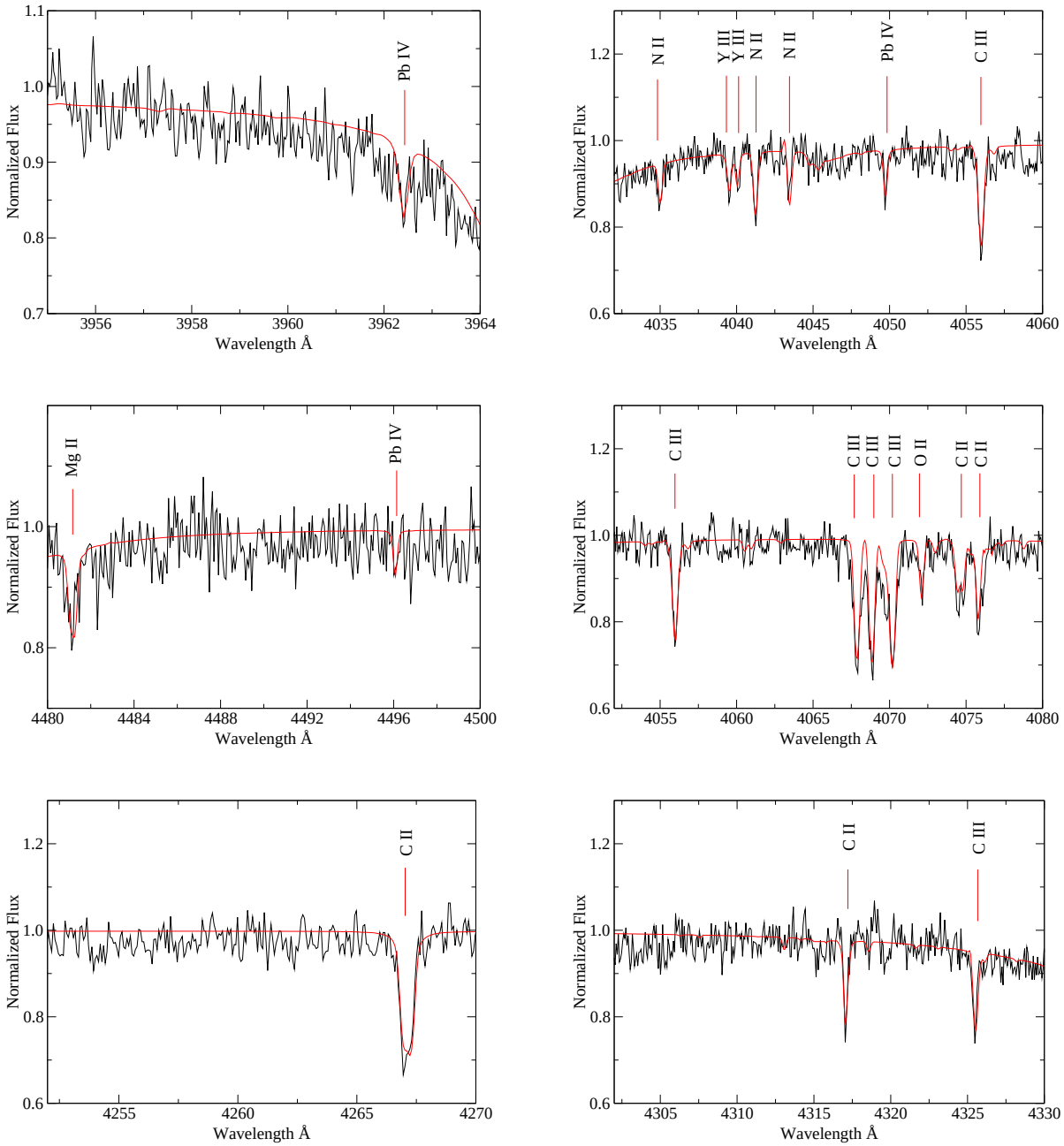

Figure 3. Segments of the VLT UVES spectrum of HE 2359–2844, together with the best-fit model, showing CII,III, NII, OII, MgII, YIII and PbIV lines.

shown in Fig. 6. This figure also shows the mean abundances and ranges for "normal" sdB stars (Pereira 2011) and other helium-rich sdB stars Naslim et al. (2010, 2011).

5 EVOLUTIONARY STATUS AND DIFFUSION IN HELIUM-RICH HOT SUBDWARFS

The question posed at the outset was to establish the relationship between the extreme-helium, the intermediate-helium and the normal hot subdwarfs. With new data from nine additional stars in the intermediate class we can make some useful observations.

The first task is to establish whether the intermediate and extreme-helium subdwarfs form a single continuum, or a number of distinct classes. Figure 7 shows the carbon-to-nitrogen ratio as a function of helium-to-hydrogen ratio for all stars analysed to date. It was already evident that the extreme helium subdwarfs appear to form carbon-rich and carbon-poor groups (Ströer et al. 2007; Hirsch 2009); this conclusion is further supported by (Németh et al. 2012, Fig. 9f). In the double-white dwarf merger model, the dis-

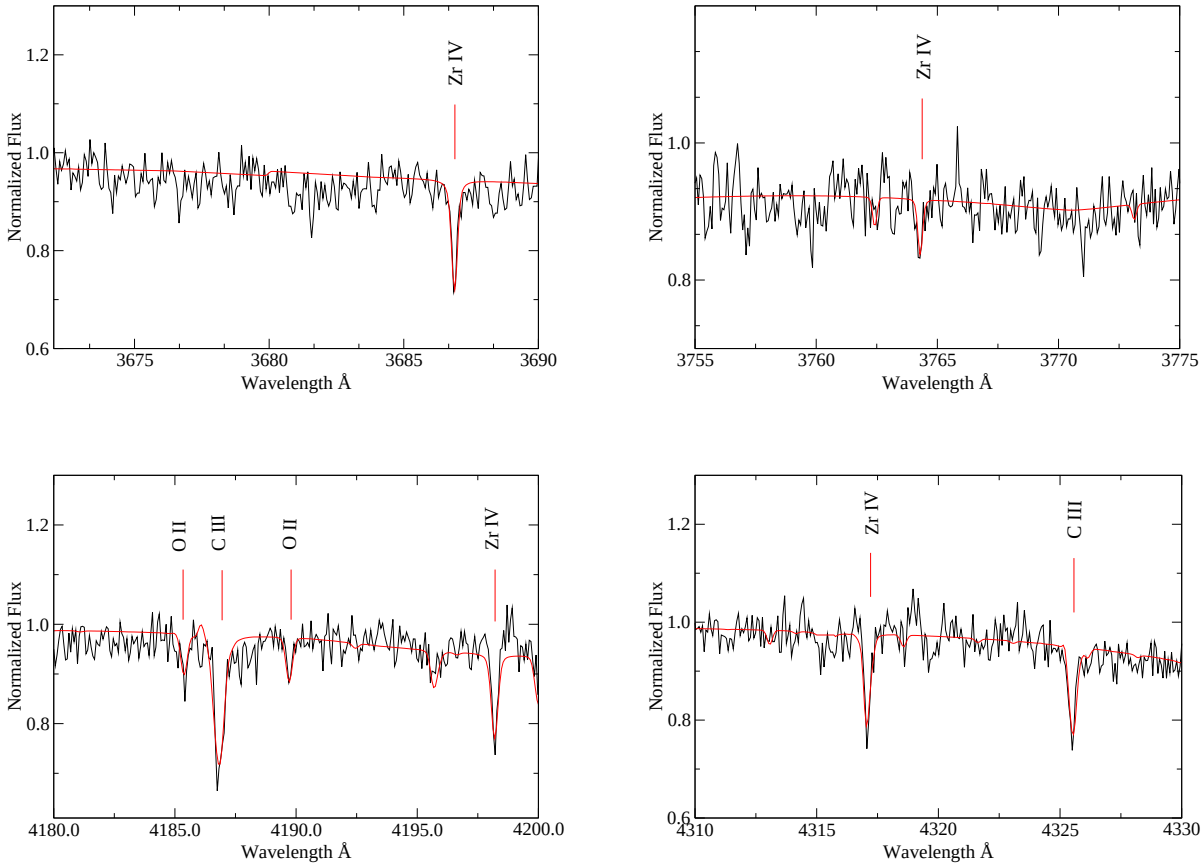

Figure 4. Segments of the VLT UVES spectrum of HE 2359–2844, together with the best-fit model, showing CIII, OII and ZrIV lines.

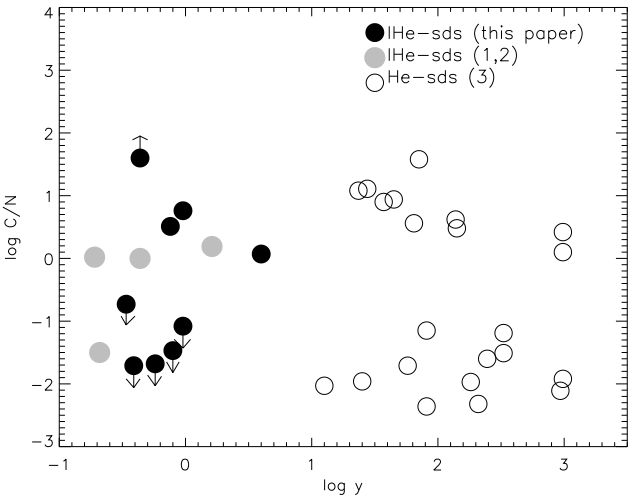

Figure 7. Carbon to nitrogen abundance ratio (n_C/n_N) as a function of helium abundance ($y \equiv \log n_{He}/n_H$) in helium-rich subdwarfs. This plot includes abundances from 1. Naslim et al. (2011, 2012), 2. Ahmad et al. (2007), 3. Hirsch (2009). Stars where carbon (or nitrogen) is not observed are represented by upper (or lower) limits.

tinction can be directly attributed to mass, the carbon-rich subdwarfs having masses $> 0.7 M_\odot$ (Zhang & Jeffery 2012).

Amongst the intermediate-helium subdwarfs, there is less evidence for two distinct classes in terms of C/N ratio. The absence of carbon or nitrogen lines in some cases is a problem which needs to be addressed using higher-quality data.

Németh et al. (2012) describe a group of He-sdO's with $0 < \log y < 1$ and $T_{\rm eff} > 40\,000$ K. Most of our stars have $-1 < \log y < 0.5$ and $T_{\rm eff} \leq 40\,000$ K; most do lie to the right of 38 000 K boundary shown in Németh et al. (2012) (Fig. 6), but in the sparsely populated region between the normal sdBs and He-sdOs. The Németh et al. (2012) sample is compared with our own in our Fig. 8. Systematic differences between the methods of analysis will have some influence; these should be comparable in magnitude with the differences noted in Table 2 between our results and those of Ströer et al. (2007). Note how the inclusion of the intermediate helium-rich subdwarfs strengthens parallels drawn between the $\log y - T_{\rm eff}$ diagram and the helium class – spectral type diagram in the hot subdwarf classification described by Drilling et al. (2013).

It is evident that some of these *intermediate* helium-rich stars are extremely peculiar. As far as we can tell, HE 2359–2844 and HE 1256–2738 are the most lead-rich stars known to science. LS IV−14°116 shows 4 dex overabundances in zir-

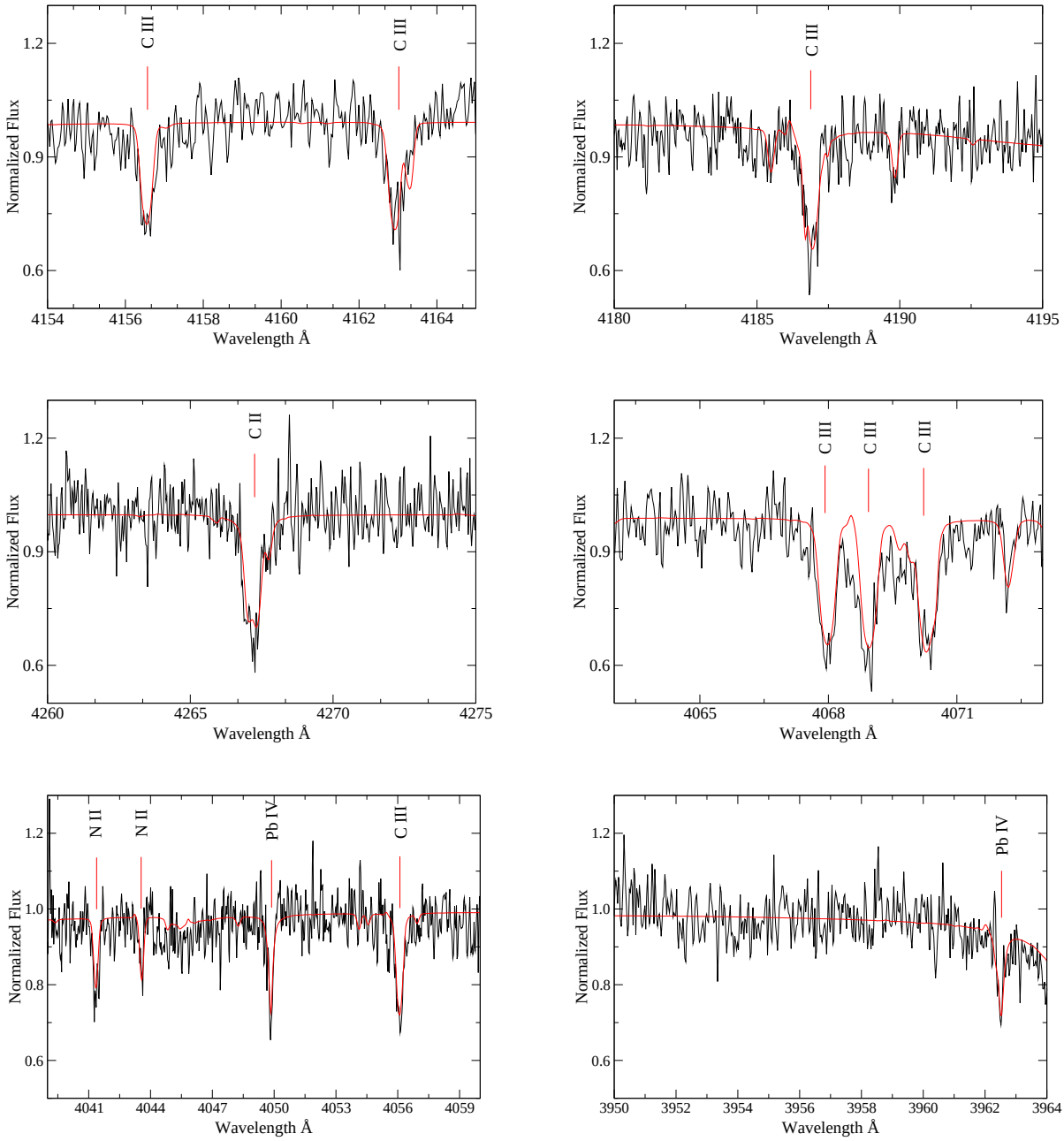

Figure 5. Segments of the VLT UVES spectrum of HE 1256–2738, together with the best-fit model, showing CIII, NII and PbIV lines.

conium, strontium, and yttrium (and 3 dex in germanium) (Naslim et al. 2011). Not having reached the thermally-pulsing asymptotic giant branch, a nuclear origin for the excess in these s-process elements appears unlikely. This leaves radiatively-driven diffusion as a favoured explanation since it is theoretically capable of concentrating particular species into a thin line-forming layer of the photosphere.

Geier (2013) reports metal abundances for a large sample of normal subdwarf B stars. In general and with some dependence upon effective temperature, most elements heavier than helium and lighter than calcium, but excepting nitrogen, are depleted by a factor ≈ 10 relative to solar. Elements heavier than and including calcium are enhanced by a similar amount, excepting iron, which is solar, and vanadium, which is > 3 dex enhanced. The intermediate helium-rich sdB stars UVO 0512–08 and PG 0909+276, analysed by Edelmann (2003), show > 3 dex overabundances in scandium, titanium, vanadium, manganese and nickel. Other elements (Ga, Sn, Pb) have been measured as > 2 dex overabundant in normal sdB stars (O'Toole & Heber 2006) using ultraviolet spectroscopy.

Calculations of the evolution of horizontal-branch stars including radiatively-driven diffusion by Michaud et al. (2011) reproduce moderately well the surface abundances of normal sdB stars (their Fig. 5), at least for elements included in the opacities (Iglesias & Rogers 1996). Diffusion

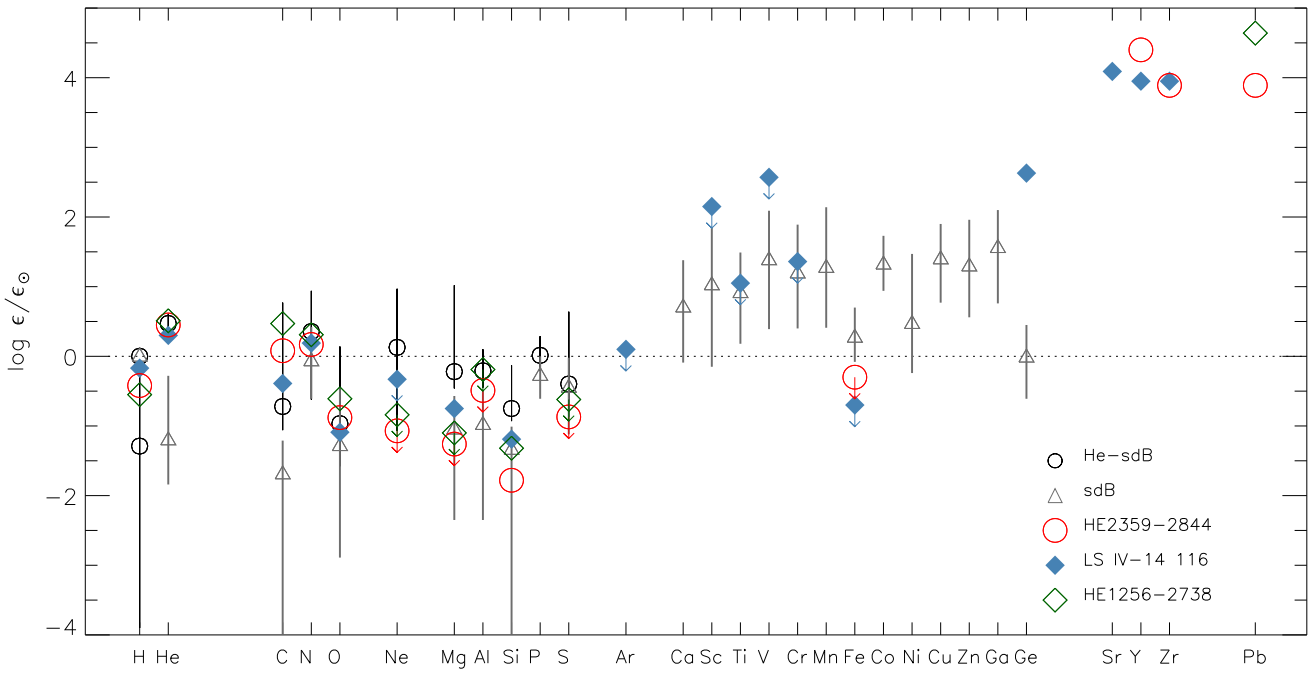

Figure 6. Elemental abundances for HE 2359–2844, HE 1256-2738 and LS IV−14°116 relative to solar values. Abundances for He-sd's (Naslim et al. 2010, 2011) and normal sdBs (Pereira 2011) are indicated by a mean (symbol) and range (line).

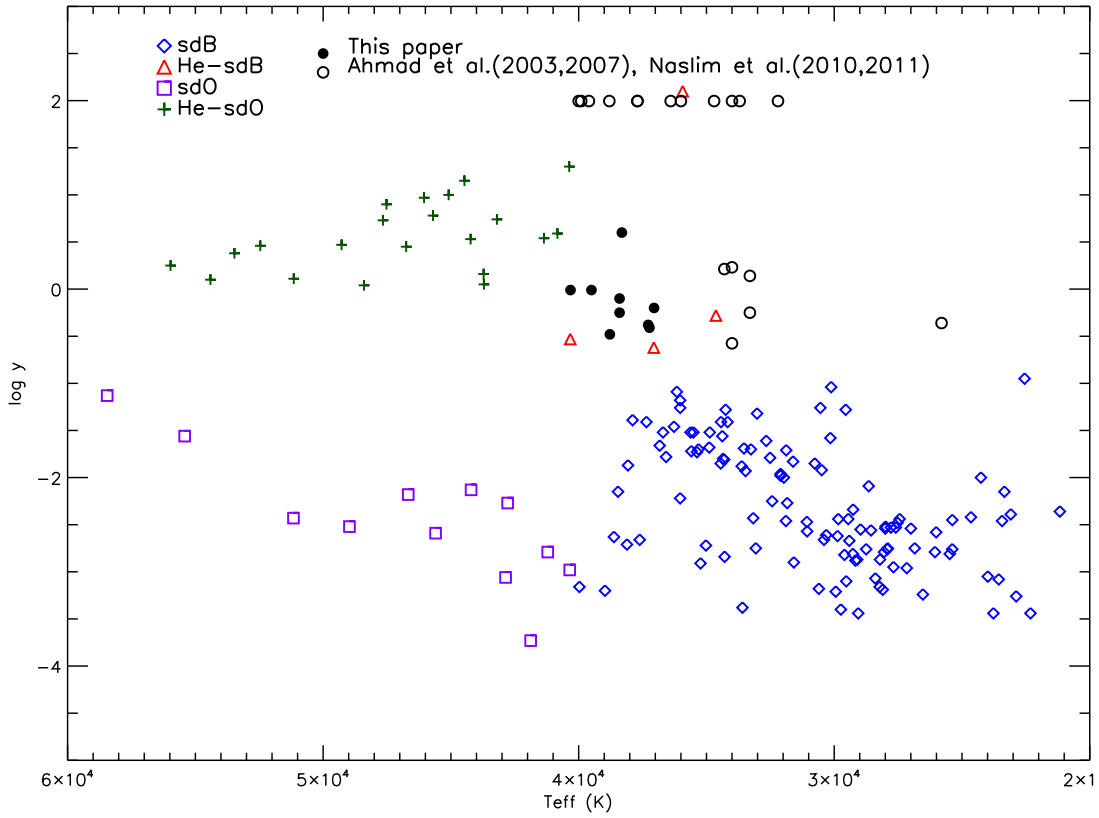

Figure 8. Helium abundance ($\log y$) as a function of effective temperature for subdwarfs analysed by Németh et al. (2012), and for intermediate helium subdwarfs analyzed by us in the present paper and previously, as indicated. Extreme helium-rich subdwarfs for which the hydrogen abundance is below the detection threshold are shown with $\log y = 2$.

calculations for most elements observed with excessive overabundances (*e.g.* Ge, Sr, Y, Zr, Sn and Pb) are not yet possible. The Michaud et al. (2011) calculations, however, represent equilibrium abundances for stars established on the (extreme) horizontal branch (EHB). Most intermediate helium-rich sdB stars lie above the classical EHB, possibly because they are evolving onto *or* away from a stable core-helium-burning configuration. In either case, the equilibrium result may not be valid. For example, Hu et al. (2011) computes a time-dependent model which demonstrates that it takes 3000 years or so after radiative levitation commences for the surface layer chemistry to stabilise, whilst Groth et al. (1985) suggest that increased photospheric mixing and helium enrichment occurs as a hot subdwarf evolves away from the extended horizontal branch.

It could be argued that stars having excessive overabundances of selected elements provide evidence for stratification immediately following onset of conditions which allow radiative levitation to operate, *i.e.* on approach to the EHB. In the absence of detailed calculations, it could also be argued that, as a star evolves away from the EHB, photospheric conditions may change sufficiently for established concentrations to rise (or sink) into the line-forming region.

In this context, one might ask whether there is some "sweet spot" in effective temperature and surface gravity where particular elemental overabundances are likely? So far, the evidence is weak; LS IV−14°116 is 3 000 K cooler than HE 2359–2844 but shows a similar zirconium abundance, whilst the two lead-rich stars also differ in effective temperature by 3 000 K. Consequently, there must be additional factors, such as age or mass, which lead to the formation of a "heavy metal" star.

6 CONCLUSION

We have analysed high-resolution spectra of nine intermediate helium-rich hot subdwarfs, having helium-to-hydrogen ratios between 0.5 and 5 (by number). In terms of carbon and nitrogen abundances and unlike the more extreme helium-rich subdwarfs, we do not find evidence of separate carbon- and nitrogen-rich groups.

Two stars, HE 2359–2844 and HE 1256–2738, show absorption lines due to triply ionized lead (Pb IV) which have never previously been detected in any star. From these lines, we have measured an atmospheric abundance of lead which is nearly ten thousand times that measured in the Sun. To our knowledge, these are the most lead-rich stars known to science.

The lead abundance is also ten to 100 times that previously measured in normal hot subdwarf atmospheres from ultraviolet spectroscopy. HE 2359–2844 also shows zirconium and yttrium abundances similar to those in the zirconium star LS IV−14°116. The best physical explanation for the large overabundances in these stars is that selective radiative forces levitate and concentrate specific ions into thin layers in the photosphere; these layers should coincide with regions where the specific opacity of an ion has a maximum value. Where high concentrations coincide with the line-forming layer, overabundances will be observable.

Extreme overabundances are only seen in intermediate helium-rich subdwarfs, which are themselves intrinsically rare and overluminous compared with normal subdwarfs. The latter are stable helium-core-burning stars with helium-poor surfaces. This suggests an association between the process that transforms a helium-poor subdwarf into an intermediate helium-rich subdwarf (or vice versa) *and* the process that produces excessive overabundances of exotic elements. We suggest that organized stratification of the atmosphere is more likely to occur during transition from a new-born helium-rich subdwarf to a normal helium-poor subdwarf.

ACKNOWLEDGMENTS

The Armagh Observatory is funded by a grant from the Northern Ireland Dept of Culture, Arts and Leisure.

REFERENCES

Ahmad A., Behara N. T., Jeffery C. S., Sahin T., Woolf V. M., 2007, A&A, 465, 541
Ahmad A., Jeffery C. S., 2003, A&A, 402, 335
Ahmad A., Jeffery C. S., 2004, A&A, 413, 323
Ahmad A., Jeffery C. S., 2006, Baltic Astronomy, 15, 139
Alonso-Medina A., Colon C., Porcher P., 2011, Atomic Data and Nuclear Data Tables, 97, 36
Asplund M., Grevesse N., Sauval A. J., Scott P., 2009, ARA&A, 47, 481
Ballester P., Modigliani A., Boitquin O., Cristiani S., Hanuschik R., Kaufer A., Wolf S., 2000, The Messenger, 101, 31
Behara N. T., Jeffery C. S., 2006, A&A, 451, 643
Christlieb N., Wisotzki L., Reimers D., Homeier D., Koester D., Heber U., 2001, A&A, 366, 898
Cowan R., 1981, The theory of atomic structure and spectra. University of California Press, Berkeley.
Drilling J. S., Jeffery C. S., Heber U., Moehler S., Napiwotzki R., 2013, A&A, 551, A31
Edelmann H., 2003, PhD thesis, Friedrich-Alexander-Universität Erlangen-Nürnberg
Edelmann H., Heber U., Hagen H.-J., Lemke M., Dreizler S., Napiwotzki R., Engels D., 2003, A&A, 400, 939
Epstein G. L., Reader J., 1975, Opt. Soc. Am, 65, 310
Geier S., 2013, A&A, 549, A110
Green R. F., Schmidt M., Liebert J., 1986, ApJS, 61, 305
Groth H. G., Kudritzki R. P., Heber U., 1985, A&A, 152, 107
Heber U., 1986, A&A, 155, 33
Heber U., 2009, ARA&A, 47, 211
Hirsch H., 2009, PhD thesis, Universität Erlangen-Nürnberg
Hirsch H., Heber U., 2009, Journal of Physics Conference Series, 172, 012015
Hu H., Tout C. A., Glebbeek E., Dupret M.-A., 2011, MNRAS, 418, 195
Iglesias C. A., Rogers F. J., 1996, ApJ, 464, 943
Jeffery C. S., Aznar Cuadrado R., 2001, A&A, 378, 936
Jeffery C. S., Woolf V. M., Pollacco D. L., 2001, A&A, 376, 497
Kramida A., Ralchenko Y., Reader J., NIST ASD Team. 2012, Technical report, NIST Atomic Spectra Database

(ver. 5.0). National Institute of Standards and Technology, Gaithersburg, MD.
Lisker T., Heber U., Napiwotzki R., Christlieb N., Reimers D., Homeier D., 2004, Ap&SS, 291, 351
Michaud G., Richer J., Richard O., 2011, A&A, 529, A60+
Moehler S., de Boer K. S., Heber U., 1990, A&A, 239, 265
Napiwotzki R., Christlieb N., Drechsel H., Hagen H.-J., Heber U., Homeier D., Karl C., Koester D., Leibundgut B., Marsh T. R., Moehler S., Nelemans G., Pauli E.-M., Reimers D., Renzini A., Yungelson L., 2001, Astronomische Nachrichten, 322, 411
Naslim N., Geier S., Jeffery C. S., Behara N. T., Woolf V. M., Classen L., 2012, MNRAS, 423, 3031
Naslim N., Jeffery C. S., Ahmad A., Behara N. T., Şahìn T., 2010, MNRAS, 409, 582
Naslim N., Jeffery C. S., Behara N. T., Hibbert A., 2011, MNRAS, 412, 363
Németh P., Kawka A., Vennes S., 2012, MNRAS, 427, 2180
O'Toole S. J., 2004, A&A, 423, L25
O'Toole S. J., Heber U., 2006, A&A, 452, 579
Pereira C., 2011, PhD thesis, Queen's University Belfast
Reader J., Acquista A., 1997, Opt. Soc. Am. B, 14, 1328
Safronova U. I., Johnson W. R., 2004, Phys. Rev. A, 69, 052511
Ströer A., Heber U., Lisker T., Napiwotzki R., Dreizler S., Christlieb N., Reimers D., 2007, A&A, 462, 269
Werner K., 1986, A&A, 161, 177
Werner K., Deetjen J. L., Dreizler S., Nagel T., Rauch T., Schuh S. L., 2003, in Hubeny I., Mihalas D., Werner K., eds, Stellar Atmosphere Modeling Vol. 288 of Astronomical Society of the Pacific Conference Series, Model Photospheres with Accelerated Lambda Iteration. p. 31
Zhang X., Jeffery C. S., 2012, MNRAS, 419, 452

APPENDIX A: ATOMIC DATA

In our previous paper (Naslim et al. 2011), we discussed several lines of Zr IV, including

4198.26 Å: 5d ^{2}D$_{5/2}$ – 6p ^{2}P$^o_{3/2}$
4317.08 Å: 5d ^{2}D$_{3/2}$ – 6p ^{2}P$^o_{1/2}$.

We now need atomic data for two further lines:

3686.90 Å: 6p ^{2}P$^o_{3/2}$ – 6d ^{2}D$_{5/2}$
3764.31 Å: 6d ^{2}D$_{5/2}$ – 6f ^{2}F$^o_{7/2}$

For the first of these new transitions, we were able to make use of the wave functions obtained in calculating data for the previously studied transitions, since the 6p levels were again included and the 6d orbital function was in fact optimised on the energy of the 6d ^{2}D state, even though it was introduced to provide some valence shell correlation for the 5d – 6p transitions. Here we augmented the 4s^{2}4p^{6}6d configuration by the configurations 4s^{2}4p^{2}4d^{2}6d and 4s4p^{6}4d6d, in parallel with the configurations introduced for the 4d and 5d states.

The second of the new transitions required the generation of 4f, 5f, 6f orbitals. We found that if we generated the orbitals using only these three configurations, there was significant mixing between them when correction configurations were added. So in our optimisation, we incorporated the main correlation configurations as well as the dominant configurations which are of the form 4s^{2}4p^{6}nf. Additionally, we optimised 7f on the 4s^{2}4p^{6}7f ^{2}F^o state, to allow for further valence shell correlation.

In the final calculations, we used the following sets of configurations:

Even parity : 4s^{2}4p^{6}nd, (4 ≤ n ≤7)
4s^{2}4p^{4}4d^{2}nd, (4 ≤ n ≤7)
4s4p^6(4dnd + kpmp),
(4 ≤ n ≤7, 5 ≤ k,m ≤ 8)
4s^{2}4p^5(4d5p+4d6p+4dnf), (4 ≤ n ≤7)

Odd parity : 4s^{2}4p^6(5p+6p+nf), (4 ≤ n ≤7)
4s^{2}4p^{4}4d^2(5p+6p+nf), (4 ≤ n ≤7)
4s4p^6(4dmp+4dnf + kp*l*d),
(m=4,5; 4 ≤ n ≤7; 5 ≤ k ≤ 8); *l*=5,6)
4s^{2}4p^{5}4dnd, (4 ≤ n ≤7)

The calculated atomic data for the two key transitions are as follows:

Wavelength (Å)	Transition	f_l	gf
3686.90	6p ^{2}P$^o_{3/2}$ – 6d ^{2}D$_{5/2}$	1.3938	5.575
3764.31	6d ^{2}D$_{5/2}$ – 6f ^{2}F$^o_{7/2}$	0.5098	3.059

where f_l is the oscillator strength, calculated in length form, and the g of gf is the (2J+1) value of the lower level of the transition. These data are calculated with experimental energies, as given by NIST. The calculated transition energies are within 2% of the experimental values. In view of this, and of the close agreement between the length and velocity forms of the oscillator strengths, we anticipate that these data should be correct to within about 10%.

For this paper, we additionally required oscillator strengths for a number of lines of Pb IV not previously observed in any star. Recent calculations of these quantities have been carried out by Safronova & Johnson (2004) and Alonso-Medina et al. (2011). The former carried out a Many-Body Perturbation Theory (MBPT) calculation, based on single and double excitations of Dirac-Fock orbitals, whilst the latter give results obtained using the relativistic Hartree-Fock method (Cowan 1981). The two sets of results differ by about a factor of two. We have chosen to use the third-order MBPT values for several reasons: first, the MBPT method has proved in general to be of greater accuracy; second, if we take as an example the line at λ3963.5, Safronova & Johnson (2004) attribute this to a one-electron 6d–7p transition, whereas Alonso-Medina et al. (2011) attribute it to a two-electron 5d^{10}6d – 5d^{9}6s6p transition; since the dipole operator involved in evaluating f-values is a one-electron operator, substantial configuration mixing would be required for this latter assignment, and this doesn't seem likely.